Marine Chemistry 244 (2022) 104136

Contents lists available at ScienceDirect

Marine Chemistry

journal homepage: www.elsevier.com/locate/marchem

Controls on surface distributions of dissolved organic carbon and nitrogen in the southeast Pacific Ocean

Mariana B. Bif [a,*], Annie Bourbonnais [b], Dennis A. Hansell [c], Julie Granger [d], Holly Westbrook [b], Mark A. Altabet [e]

[a] Monterey Bay Aquarium Research Institute (MBARI), Moss Landing, CA, USA
[b] School of the Earth, Ocean and Environment, University of South Carolina, Columbia, SC, USA
[c] Department of Ocean Sciences, Rosenstiel School of Marine and Atmospheric Sciences (RSMAS), University of Miami, Miami, FL, USA
[d] Department of Marine Sciences, University of Connecticut, CT, USA
[e] School for Marine Science and Technology, University of Massachusetts Dartmouth, New Bedford, MA, USA

ARTICLE INFO

Keywords:
Biogeochemical cycles
Dissolved organic matter
Dissolved organic nitrogen
Nitrogen isotopes
Subtropical gyres

ABSTRACT

Here we use data from three meridional survey cruises that took place in 1994, 2007/2008 and 2016/2017 in the southeast Pacific Ocean to investigate controls on surface distributions of dissolved organic carbon and nitrogen (DOC and DON, respectively). While DOC and DON production occur simultaneously in the euphotic layer of the gyre margins, budgets that account for horizontal transport, production and consumption are not balanced across the region. Our results show that while DOC concentrations increase inside the gyre, DON remains at similar levels in comparison to margins. There is little interannual variability in DOC and DON trends, except near the equator, explained by ENSO phases and seasonality. While the effect of evaporation (precipitation) did not significantly contribute to variable DOC and DON concentrations, differences in the naturally occurring $^{15}N/^{14}N$ isotope ratios from the most recent cruise suggest net consumption of allochthonous DON inside the gyre. In the northernmost and southernmost stations, where surface [NO_3^-] was detected, ^{15}N-DON showed low signatures in the upper 300 m of 3.8 ± 1.5‰ and 2.5 ± 1.6‰, respectively. Inside the gyre where [NO_3^-] was undetectable, higher values averaging 5.0 ± 0.9‰ were observed. This suggests that a fraction of DON turns over more rapidly than the time scale of horizontal transport, with the isotopic change reflecting the gradient in ^{15}N-DON of newly produced organic matter. Thus, allochthonous DON is likely a significant source of nitrogen to microbial communities inside this nitrogen-limited environment and should be taken into consideration when closing nutrient budgets to estimate productivity in the South Pacific Subtropical Gyre.

1. Introduction

Marine production of dissolved organic matter (DOM) occurs at greatest rates in equatorial and coastal systems resulting from enhanced primary production (PP). DOM is composed of an array of different molecules with varying bioreactivity (McCarthy et al., 1998; Berman and Bronk, 2003; Repeta, 2015). A fraction of freshly produced DOM is not readily consumed by local phytoplankton and microbes, thereby accumulating in the euphotic layer to be subsequently advected far from production sites following ocean circulation (Hansell and Carlson, 1998; Roussenov et al., 2006; Charria et al., 2008; Hansell et al., 2009; Letscher et al., 2013; Carlson and Hansell, 2015; Santinelli et al., 2021). Recalcitrant dissolved organic carbon (DOC) can survive degradation for months to millennia and its surface distribution is often linked with the distribution of conservative properties such as temperature and salinity (Hansell and Waterhouse, 1997; Siegel et al., 2002). In the tropics, freshly produced DOC is advected from the productive zones toward the center of subtropical gyres (Thingstad et al., 1997; Raimbault et al., 2007; Hansell et al., 2009; Carlson and Hansell, 2015).

Elevated [NO_3^-] in productive regions supports enhanced PP that in turn increases surface [DON] (Bronk and Ward, 1999; Ward and Bronk, 2001; Bronk and Ward, 2005; Letscher et al., 2013), but DON concentrations remain unchanged or slightly decrease inside gyres and in western boundaries. For this reason, these distant sites are assumed to be sinks for advected DON, meeting local heterotrophic (i.e., DON remineralization) and autotrophic (i.e., assimilation of remineralized DON)

* Corresponding author.
E-mail address: marianabif@gmail.com (M.B. Bif).

https://doi.org/10.1016/j.marchem.2022.104136
Received 6 December 2021; Received in revised form 23 May 2022; Accepted 30 May 2022
Available online 5 June 2022

nitrogen requirements in the absence of other sources. Previous studies in the North Atlantic Ocean suggest that nitrate introduced by Ekman transport (Williams and Follows, 1998) and lateral DON inputs (Bronk et al., 2007; Charria et al., 2008) stimulate primary production inside that gyre, and that DON contributes to close the budget of total particle export (Roussenov et al., 2006). A study conducted along a broad meridional section of the South Pacific Subtropical Gyre (SPSTG) investigated the controls on total organic carbon (TOC) and nitrogen (TON) surface distributions, hypothesizing that while TOC is strongly controlled by physical processes such as lateral advection, TON must be controlled by biological consumption and subsequent export (Hansell and Waterhouse, 1997). This hypothesis was supported by an inverse circulation modelling approach, which diagnosed that DON is supplied laterally to the gyre from the eastern and equatorial regions, stimulating PP therein, and closing the nitrogen budget requirements for the observed net primary productivity (Letscher et al., 2016).

The SPSTG is an ultra-oligotrophic system that contains the lowest chlorophyll levels among the world's oceans (Morel et al., 2010) owing to the limited supply of nitrogen and iron to the sunlit surface (Behrenfeld and Kolber, 1999; Moore et al., 2013). In contrast to the North Pacific and Atlantic subtropical gyres, nitrogen fixation is negligible in the eastern portion of the gyre (Knapp et al., 2016). DON removal inside this gyre occurs following at least two main mechanisms: DON is either 1) removed via consumption in the surface ocean and exported as sinking particles (Knapp et al., 2018) or 2) removed following vertical mixing of the upper water column and consumed by upper mesopelagic microbes (Letscher et al., 2013, 2016). Although DON represents a N source for marine microbial communities in oligotrophic gyres (Seitzinger and Sanders, 1999; Bradley et al., 2010; Kujawinski, 2011; Letscher et al., 2013; Knapp et al., 2018), its role in sustaining PP is still unclear as observations are limited such as in the eastern portion of the South Pacific Ocean, the subject of this work. Additionally, changes in [DON] are subtle against the background concentration, and thus should not serve as the sole evidence of biological activity (Knapp et al., 2018).

Stable isotope ratios of nitrogen in DON, $^{15}N/^{14}N$, provide a sensitive tool to verify whether DON is imported to the gyre surface from the productive margins and consumed therein, and can be applied to investigate processes involving DON production in the margins and its subsequent consumption inside the gyre (Knapp et al., 2005; Meador et al., 2007; Bourbonnais et al., 2009; Knapp et al., 2018). ^{15}N-DON measurements in a zonal transect along the Eastern Tropical South Pacific between 10°S-20°S and 80°W-100°W have intimated that DON production is decoupled from immediate uptake, and its advection from the eastern margin toward the gyre with subsequent consumption alleviates local nitrogen limitation and supports export production (Knapp et al., 2018). These processes were observable by measuring isotopic signatures in the upper ocean (Knapp et al., 2011). While production adds surface DON with a relatively low $\delta^{15}N$ (‰ versus air), consumption acts to increase the $\delta^{15}N$ of DON due to kinetic isotopic fractionation – this was also observed in the South China Sea (Zhang et al., 2020). However, broad regions of the South Pacific Ocean still lack such isotopic observations, limiting our ability to fully assess DON advection from the other productive margins and its support to biological activity within the gyre.

Here we assess biogeochemical data from three meridional cruises that crossed the eastern South Pacific Ocean (between 5°S-40°S along ~103°W in 1994, 2008 and 2017) to further our understanding of controls on DOC and DON surface distributions and observe whether there is interannual variability. For the most recent cruise (2017), we analyzed $\delta^{15}N$-DON isotopes to test if biological processes regulate DON distribution along the pathway between production sites (i.e., equatorial upwelling ~5°S and the subtropical front ~40°S) and the center of the SPSTG. We also analyzed $\delta^{15}N\text{-}NO_3^-$ from the 2008 and 2017 cruises when NO_3^- concentrations were $> 0.1\ \mu M\ kg^{-1}$. DON isotopic signatures are associated with local $\delta^{15}N\text{-}NO_3^-$ signatures if NO_3^- is a significant nitrogen source for DON production (Altabet, 1988; Knapp et al., 2005; Knapp et al., 2011; Knapp et al., 2016; Knapp et al., 2018). The ultra-oligotrophic SPSTG, where surface $[NO_3^-]$ is undetectable in the center and the nitracline is significantly deeper than the mixed layer, provides suitable conditions to test the hypothesis that allochthonous DON is a nitrogen source for microbial communities inside the gyre.

2. Material and methods

2.1. Study area and regional hydrography

The study area encompasses an eastern meridional section of the South Pacific Ocean where three occupations of the P18 section were conducted in years 1994, 2007/2008 and 2016/2017 as part of the U.S. World Ocean Circulation Experiment, U.S. Repeat Hydrography Program and U.S. GO-SHIP, respectively. The full cruises departed from San Diego, United States, reached the Southern Ocean and then sampled northeastward until offshore of the entrance to the Strait of Magellan (in 1994 this route was reversed, traveling from south to north). To focus on the region associated with the SPSTG, we limited our study to the subsection between 5°S and 40°S (Fig. 1). The northernmost station was located at 110°W; the transect then shifted southeastward until 10°S, 103°W and from this latitude, sampling to the south followed the same longitude.

The P18 subsections crossed an extensive portion of the eastern South Pacific Ocean, from a high-nutrient low-chlorophyll (HNLC) region north of ~15°S underlain by an intense OMZ north of one of the

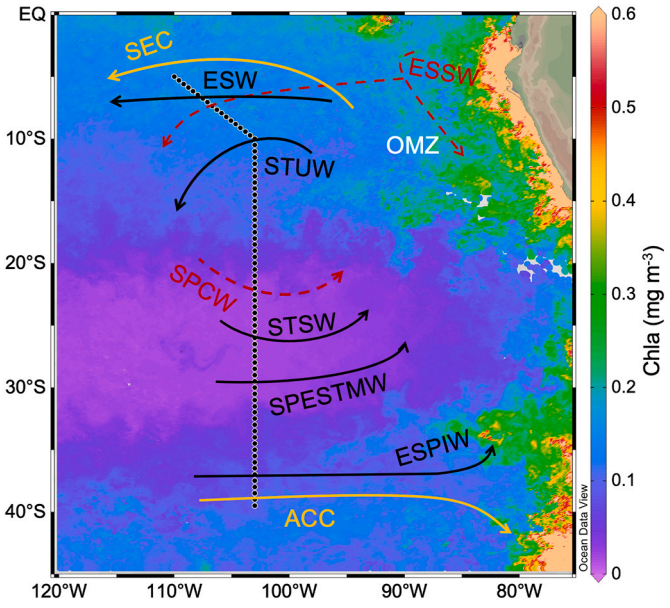

Fig. 1. Map of the study area showing the P18 subsection over mean surface chlorophyll *a* concentration for the year of 2016 (MODIS-Aqua monthly resolution, available at https://giovanni.gsfc.nasa.gov/giovanni). Each black dot represents one sampling point during the 2016–2017 cruise. The South Equatorial Current (SEC) and Antarctic Circumpolar Current (ACC) delimit the northernmost and southernmost stations, respectively, and are shown as yellow arrows. Black continuous arrows schematically represent the upper layer circulation of water masses: Equatorial Surface Water (ESW), Subtropical Surface Water (STSW), Subtropical Underwater (STUW), South Pacific Eastern Subtropical Mode Water (SPESTMW) and Eastern South Pacific Intermediate Water (ESPIW). Red dashed arrows represent the local circulation of subsurface water masses: South Pacific Central Water (SPCW) and East Equatorial Subsurface Water (ESSW); see Fig. 2 below for water mass depth distribution along the transect and Table 2 for water mass definitions. The location of the major oxygen minimum zone (OMZ) in the Eastern Tropical South Pacific is also referenced in the map. (For interpretation of the references to colour in this figure legend, the reader is referred to the web version of this article.)

most oligotrophic regions in the ocean (Fig. 1), with the deepest nutricline of about 150 m near 20°S. As such, characterizing the regional hydrography is necessary for proper data interpretation. To describe the biogeochemical processes occurring in the upper ocean within the mixed layer, we first consider the water masses and regional circulation patterns for the upper 300 m depth. This depth interval lies deeper than the mixed layer and main thermocline where vertical exchanges between the surface and subsurface waters modulate primary production, subsequently affecting DOC and DON concentrations. For water mass identification, we followed the descriptions and nomenclature in the literature (Wyrtki, 1966; Oberhuber, 1988; Sprintall and Tomczak, 1993; O'Connor et al., 2002; Karstensen, 2004; Wong and Johnson, 2003; O'Connor et al., 2005; Fiedler and Talley, 2006; Silva et al., 2009; Qu et al., 2013; Montes et al., 2014; Peters et al., 2018; Villa-Alfageme et al., 2019; and references therein). Each water mass was characterized according to its physical and chemical characteristics at the time of formation, acknowledging mixing along the pathways, and were then described in the local circulation context.

2.2. Repeat hydrography cruises: core variables

The following core variables were included in this study and employed to calculate derived variables: temperature (°C), salinity, dissolved oxygen (DO; μmol kg^{-1}), dissolved organic carbon (DOC; μmol kg^{-1}), total dissolved nitrogen (TDN; μmol kg^{-1}), nitrate (μmol kg^{-1}) and nitrite (μmol kg^{-1}). More details on the sampling protocols and chemical analysis for each parameter, together with the meta- and bottle data for each cruise, can be found at https://cchdo.ucsd.edu (I.D.s 31DSCG94_1, 33RO20071215 and 33RO20161119) and in the acknowledgements section. To investigate the biological controls on DON distribution along P18, we analyzed $\delta^{15}N$ of NO_3^- samples from 2007/2008 and 2016/2017 cruises, and $\delta^{15}N$ of DON from the 2016/2017 cruise. The analyses of chemical parameters and isotopes are detailed in the following section, and the sampling plan for each parameter per cruise is summarized in Table 1.

Temperature, salinity, DO, DOC, TDN, NO_3^- and NO_2^- were collected and analyzed for all cruises by different research groups as part of the core variables. Samples for DOC and TDN were analyzed at the Bermuda Institute of Ocean Sciences (BIOS) for the 1994 cruise (Hansell and Waterhouse, 1997), and at the University of Miami (Hansell Lab) for the 2008 (Dickson et al., 2007) and 2017 (Halewood et al., 2010) cruises. [TDN] was then used to calculate [DON], as DON (μmol kg^{-1}) = TDN – [NO_3^- + NO_2^-]. During the 1994 cruise, samples for organic carbon and nitrogen were collected unfiltered and thus contained particulate organic carbon and nitrogen. Since most of the organic carbon and organic nitrogen accumulate in the open ocean as dissolved fractions, especially in subtropical gyres (Hansell et al., 2009; Torres-Valdés et al., 2009), we refer to these parameters from 1994 as DOC and DON throughout the manuscript.

2.3. Isotopic analyses of $\delta^{15}N$-DON and $\delta^{15}N$ -NO_3^-

Subsamples from the 2017 expedition were filtered using a pre-combusted 0.7 μm GF/F filter and kept frozen in acid-cleaned polycarbonate bottles for subsequent determination of [TDN] (high-temperature combustion) and the isotopic composition of DON and NO_3^-. $\delta^{15}N$ of TDN was measured as described in Knapp et al. (2005). Briefly, TDN was oxidized to NO_3^- using recrystallized persulfate followed by NO_3^- isotope analysis with the denitrifier method (Sigman et al., 2001; Weigand et al., 2016). Only samples in which DON comprised over 40% of total TDN were included in the analysis. Six (6) mL of sample were aliquoted with 1 mL of freshly prepared persulfate oxidizing reagent (POR) in milli-Q rinsed pre-combusted, 20 mL borosilicate vials with Teflon-lined caps and aluminum seals, then autoclaved for 20 min. Pure POR concentrations were always below 3.5 μmol L^{-1}, and [TDN] concentrations were corrected for POR blanks. Prior to isotopic analysis, the pH of autoclaved samples and POR blanks was then adjusted to 2–3 with concentrated HCl, and the $\delta^{15}N$ of NO_3^- therein was measured using the denitrifier method (Sigman et al., 2001; Weigand et al., 2016). The product N_2O was purified and analyzed at the University of Connecticut using a Thermo Delta V Advantage continuous flow isotope ratio mass spectrometer equipped with a modified Thermo Gas Bench II and GC Pal autosampler. Target sample size was 7.5 nmoles. Samples were standardized using a two-point correction with the international standards IAEA-N3 ($\delta^{15}N = 4.7‰$ vs air) and USGS-34 ($\delta^{15}N = -1.8‰$ vs air). The isotope ratios are expressed in δ (‰) relative to air for N and to Vienna – Standard Mean Ocean Water (V-SMOW) for O, where $\delta^{15}N_{sample}$ and $\delta^{18}O_{sample} = (R_{sample}/R_{std} - 1)$ x 1000 and R is the isotope ratio ($^{15}N/^{14}N$ or $^{18}O/^{16}O$) measured for the sample and international standard. In samples from the 2017 cruise where [NO_3^-] represented between 10% and 60% of [TDN], $\delta^{15}N$ of NO_3^- (prior to sample oxidation) was also determined. For both 2008 and 2017 cruises, $\delta^{15}N$ of NO_3^- isotopes were determined using the denitrifier method (Sigman et al., 2001; Casciotti et al., 2002), with an average standard deviation of ±0.3‰ for $\delta^{15}N$.

The average standard deviation for triplicate $\delta^{15}N$-DON analysis was ±0.4‰. For each oxidation set, the DON oxidation efficiency was tested using 3 in-house standards (aminocaproic acid (ACA), histidine and serine) at a concentration of 10 μmol L^{-1}. The mean DON oxidation yield was 100.7 ± 5.1% for all standards ($n = 57$). Mean $\delta^{15}N$ of DON values for internal standards were 4.4 ± 0.7‰ ($n = 16$) for ACA, 2.2 ± 0.4‰ ($n = 14$) for histidine and − 4.4 ± 0.5‰ (n = 14) for serine. These values agreed well with $\delta^{15}N$ values determined by direct combustion, i.e., 4.5 ± 0.1 for ACA, 2.3 ± 0.1 for histidine and − 4.3 ± 0.1 for serine, with deviation from expected values of less than 3.6% (Zhang and Altabet, 2008).

A propagated error analysis was performed using the variance of uncertainties from $\delta^{15}N$-DON, $\delta^{15}N$-POR and $\delta^{15}N$-NO_3^- analyses (Peters et al., 1974). We acknowledge that variances associated with DON and NO_3^- concentrations also exist, however, these parameters were not analyzed in replicates and thus cannot be included in the error analysis. The propagated error for the $\delta^{15}N$-DON analysis was ≤0.51‰ with an average standard deviation of ±0.35‰ for $\delta^{15}N$. The $\delta^{15}N$ of DON was

Table 1
Number of samples collected for each variable in the upper 300 m of the water column between 5°S and 40°S, for each of the 3 occupations. Cruise ID = calendar year at the end of each cruise to be used as a reference name through the manuscript; Start and end dates = timespan in which samples were collected between 5°S and 40°S; T = temperature; DO = dissolved oxygen; DOC = dissolved organic carbon; TDN = total dissolved nitrogen.

		Number of samples collected						
Cruise ID	Start and end dates	T (°C)	Salinity	DO (μmol kg^{-1})	Nitrate (μmol kg^{-1})	Nitrite (μmol kg^{-1})	DOC (μmol kg^{-1})	TDN (μmol kg^{-1})
1994	15-Mar-1994 10-Apr-1994	677	655	638	661	661	210	173
2008	02-Jan-2008 28-Jan-2008	776	776	771	772	772	383	382
2017	10-Dec-2016 09-Jan-2017	460	460	458	368	368	221	221

determined by isotopic mass balance taking into consideration the concentration and $\delta^{15}N$ of the POR, NO_3^- and TDN. For samples where $[NO_3^-]$ was below detection limit or too low for its isotopic composition to be measured (<0.3 μM), the $\delta^{15}N$-DON is expressed as the $\delta^{15}N$-TDN minus the POR blank. Results from the isotopic analyses are compiled in the Table S1, found in the supporting information material.

2.4. Derived variables and data analysis

The calculation of derived variables and creation of figures were done using the software packages Matlab® (v.R2019a) and Ocean Data View® (ODV, v.5.2.0; Schlitzer, 2019). Mixed layer depths (MLD) were calculated using a temperature difference criterion of 0.5 °C (de Boyer Montégut et al., 2004). To calculate anomalies in physico-chemical properties between cruise years, data were first interpolated to a grid of 0.3° latitude and 20 m depth using the datafun toolbox and objmap function for Matlab® (mooring.ucsd.edu/software/matlab/doc/toolbox/datafun/index.html). In order to separate physical and biological processes controlling DOC and DON concentrations, we isolated the role of evaporation within the mixed layer by calculating salinity-normalized DOC and DON (sDOC and sDON, respectively) for the 2017 cruise. For example, sDOC was calculated using the following equation: sDOC = DOC * reference salinity / salinity (μmol kg^{-1}). Here, the reference salinity is the salinity of the main water source: for the subtropical gyre subsection between 5°S and 32°S, we applied the reference salinity of 35.23 as it is the mean surface salinity found in the core of ESW (between 5°S and 8°S). For the region >32°S we used the reference salinity of 34.2, which was found in the bottom layer of ESPIW (σ_θ = 26.6 kg m^{-3} at 40°S). This water mass then acquires a minimum salinity signature due to precipitation above σ_θ = 26.0 kg m^{-3} (Karstensen, 2004).

3. Results

3.1. Hydrography and physico-chemical properties of the upper southeast Pacific Ocean

Near the equator, the strong westward South Equatorial Current (SEC) entrains relatively fresh waters advected from the Peru Current and the equatorial upwelling system (Wyrtki, 1966; Fiedler and Talley, 2006), delimiting our northernmost stations (Fig. 1). Southward along the P18 transect, the SPSTG is delimited by the central tropical Pacific in the west, by coastal currents off Chile in the east and southeast (Fiedler and Talley, 2006; Montes et al., 2014; Peters et al., 2018) and by the eastward Antarctic Circumpolar Current (ACC) in the south (Wyrtki, 1966; Fiedler and Talley, 2006). The main water masses found in the upper 300 m were identical for all cruises and are represented here for the 2017 cruise (Fig. 2). Their physico-chemical characteristics are summarized in Table 2. Water masses from the upper thermocline are defined as having a σ_θ < 26.0 kg m^{-3} (Fig. 2b; Peters et al., 2018 and references therein). The upper thermocline was dominated by five water masses with distinctive physico-chemical properties. The Equatorial Surface Water (ESW) was found approximately between 5°S-12°S from surface to ~70 m (Fig. 2). In 2008 and 2017, the ESW was colder, saltier, and more oxygenated in comparison to 1994 (Fig.S1a-f).

The warm and salty Subtropical Surface Water (STSW) dominated the center of the gyre around 20°S at shallow depths (Fig. 2). Approximately between 12°S-27°S the upper layer was constituted by the Subtropical Underwater (STUW) that was also found below STSW. Along the P18 subsection, STUW's maximum depth was found near 200 m at 22.2°S, reaching as far as 27°S with variable temperature and salinity between cruise years (Fig.S1). Immediately beneath STUW lies the South Pacific Eastern Subtropical Mode Water (SPESTMW), blocked from air-sea exchanges by the STUW and ESW near the equator but near the

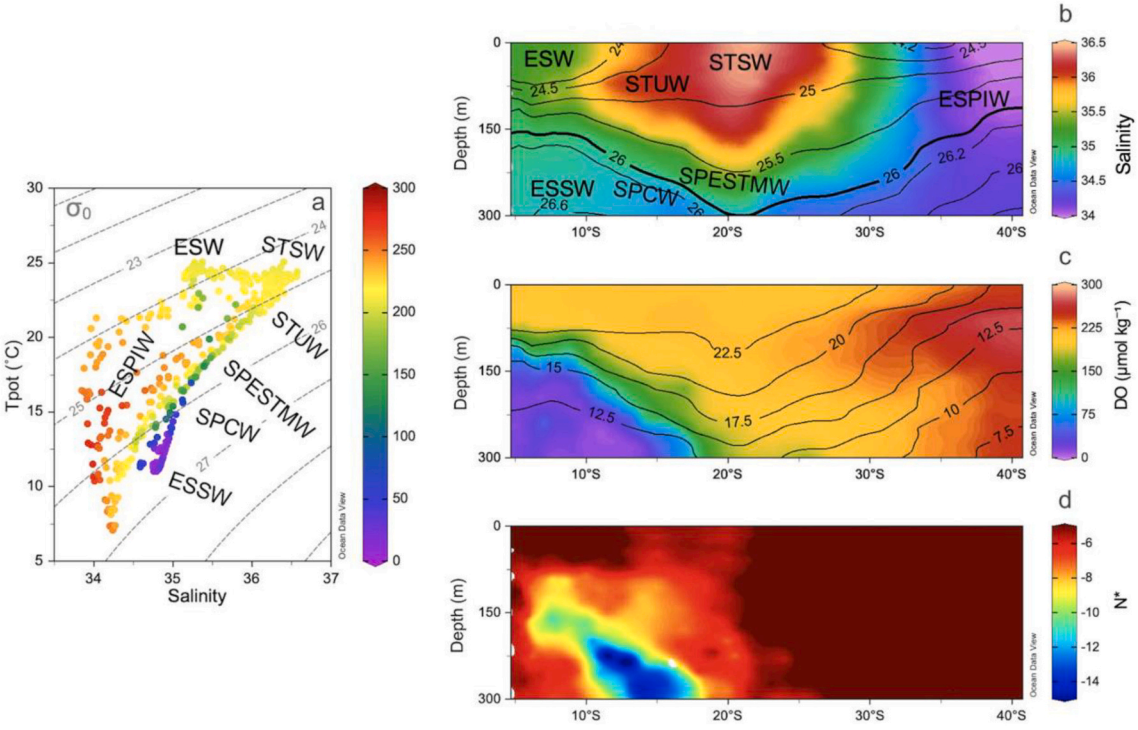

Fig. 2. P18/2017 subsection showing the physico-chemical properties for the upper 300 m of depth. (a) T/S diagram showing oxygen concentrations (z-axis; μmol kg^{-1}) of the main water masses found in this study (ESW = Equatorial Surface Water; STSW = Subtropical Surface Water, STUW = Subtropical Underwater, SPESTMW = South Pacific Eastern Subtropical Mode Water, SPCW = South Pacific Central Water, ESWW = Equatorial Subsurface Water, ESPIW = Eastern South Pacific Intermediate Water); (b) salinity section overlaid by potential density anomalies (σ_θ, kg m^{-3}) with the approximate location of the different water masses. The thick black isoline of 26 kg m^{-3} limits the upper thermocline; (c) dissolved oxygen (DO) concentrations (μmol kg^{-1}) overlaid by temperature (°C); (d) N* calculated as $[NO_3^-]$-16*$[PO_4^{3-}]$ + 2.9 (μmol kg^{-1}; Deutsch et al., 2001).

Table 2
Definitions for the water masses included in this study.

Full name	Water mass acronym	Pot-T (°C)	Salinity	σ_θ (kg m^{-3})	Other features	Latitude range	References
Equatorial Surface Water	ESW	<25	>34	<24.2		<12°S	Wyrtki, 1966; Fiedler and Talley, 2006
Subtropical Surface Water	STSW	>23	>36	<24.6		18°S-23°S	Wyrtki, 1966; Fiedler and Talley, 2006
Subtropical Underwater	STUW	>20	>36	<25.4		12°S-27°S	Oberhuber, 1988; Wong and Johnson, 2003; O'Connor et al., 2005; Qu et al., 2013
South Pacific Eastern Subtropical Mode Water	SPESTMW	16–23	34.8–36.2	25–25.7		10°S-32°S	Wong and Johnson, 2003; Fiedler and Talley, 2006; Peters et al., 2018
South Pacific Central Water	SPCW	12–15	34.5–34.8	26–26.2		15°S-35°S	Sprintall and Tomczak, 1993; Peters et al., 2018; Villa-Alfageme et al., 2019
Equatorial Subsurface Water	ESSW	10–15	34.5–35	26.2–26.6	N* < −5	5°S-17°S	Fiedler and Talley, 2006; Silva et al., 2009; Montes et al., 2014; Peters et al., 2018
Eastern South Pacific Intermediate Water	ESPIW	7.5–15	<34.5	24.5–26.8	high DO tongue	>32°S	Karstensen, 2004; Wong and Johnson, 2003; Silva et al., 2009; Peters et al., 2018

surface at depths between 27°S-32°S. South of the SPESTMW, a fresher, cold and oxygen-enriched water mass (Fig. 2) was identified as Eastern South Pacific Intermediate Water (ESPIW). In our study region, ESPIW dominated the water column at latitudes >32°S with varying oxygen concentrations between cruise years (Fig.S1g-i).

Below the main thermocline two water masses were identified far from the mixed layer boundary. South Pacific Central Water (SPCW) was observed in a limited area between 15°S and 35°S, below SPESTMW and along the 26.0 kg m^{-3} density outcrop as a low-salinity feature within the thermocline (Fig. 2 ac). The second water mass was located north of 17°S as the Equatorial Subsurface Water (ESSW). Both water masses had a strong negative N* feature, <−5 μmol kg^{-1}, due to significantly low oxygen concentrations (Fig.S1g-i). The feature was observed below 150 m depth and centered around 15°S (Fig. 2c, d) and represents the oxygen minimum zone (Silva et al., 2009). Since our study region was westward of the ESSW's main pathway, a portion of these waters must have been transported by the SEC as this low oxygen feature was previously observed as far west as 103°W (Fiedler and Talley, 2006).

3.2. Biogeochemistry of the southeast Pacific Ocean's upper water column

In general, MLDs were deeper and showed interannual variability inside the gyre, reaching the deepest extent in 2017 near 20°S (Fig. 3a). Temperatures within the mixed layer were uniform north of 25°S except in 1994, when the upper ocean was warmer between 5°S and 12°S. That latitudinal band had a mean temperature of 27.2 ± 0.6 °C in 1994 versus 23.1 ± 0.3 °C in 2007 and 24.4 ± 0.3 °C in 2017. Surface temperatures subsequently decreased at higher latitudes during all cruises (Fig. 3b).

As for nitrate distributions along the transect, surface concentrations were distinct between regions dominated by either ESW, SPSTG waters

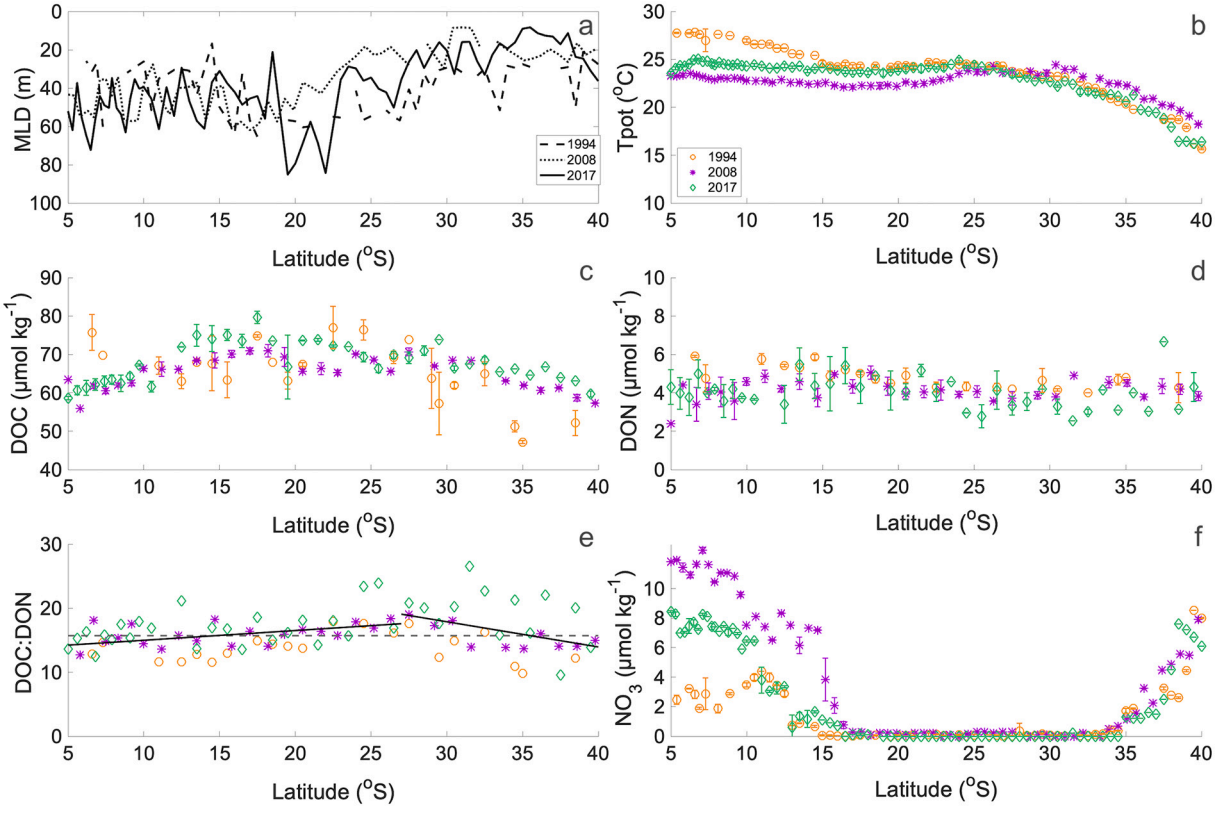

Fig. 3. Surface distribution of variables across the P18 subsection for the 1994, 2008 and 2017 cruises. Mean concentrations were estimated from values within the mixed layer ±1 standard deviation. (a) Mixed layer depth (MLD; m) ; (b) potential temperature (°C); (c) dissolved organic carbon (DOC; μmol kg^{-1}); (d) dissolved organic nitrogen (DON; μmol kg^{-1}); (e) DOC:DON ratios with mean ratio (15.7:1, dashed line) and trendlines for subsections between 5°S-27°S and 27°S-40°S (continuous lines); and (f) nitrate concentrations (μmol kg^{-1}).

or ESPIW (Fig. 3f). Near the Equator in the region dominated by ESW, NO_3^- concentrations were the highest and with significant interannual variability. In 1994, maximum [NO_3^-] averaged only 4.4 μmol kg^{-1} in the mixed layer while reaching 12.6 μmol kg^{-1} in 2008 and 8.4 μmol kg^{-1} in 2017. These values gradually decreased toward the SPSTG and were below detection limits (<0.1 μmol kg^{-1}) at about 16.5°S for all years. Surface nitrate was undetected until about 34.5°S then gradually increased southward as the subtropical front with the Southern Ocean was crossed. HNLC conditions began south of this front. At 39.5°S the upper waters were dominated by ESPIW and [NO_3^-] were similar across years, averaging 7.9 ± 0.7 μm kg^{-1}.

DOC distributions mirrored each other in 2006 and 2017 but appeared different in 1994. Waters associated with ESW north of 12°S showed similar DOC concentrations within the mixed layer in 2008 and 2017 averaging 62.3 ± 3.6 μmol kg^{-1} and 62.5 ± 2.0 μmol kg^{-1}, respectively (Fig. 3c). Concentrations were higher in 1994 averaging 70.9 ± 4.4 μmol kg^{-1}. Although we only had two stations for this region in 1994, the relatively higher [DOC] could have been associated with the SEC variability that year, given warmer conditions. Alternatively, since samples were collected unfiltered, elevated [DOC] seen in 1994 could have been attributed to organic particles near the Equator. Inside the gyre between 12°S and 27°S, [DOC] within the mixed layer was elevated for all years, averaging 69.3 ± 5.1 μmol kg^{-1} in 1994, 72.4 ± 3.5 μmol kg^{-1} in 2008 and 68.3 ± 2.1 μmol kg^{-1} in 2017. In higher latitudes South of 27°S, [DOC] within the mixed layer decreased to averages of 60 ± 9.1 μmol kg^{-1}, 63.8 ± 4.1 μmol kg^{-1} and 66.6 ± 3.7 μmol kg^{-1} in 1994, 2008 and 2017, respectively. Below the mixed layer, [DOC] gradually decreased, reaching <50 μmol kg^{-1} along the thermocline (σ_θ = 26.0 kg m^{-3}), as shown for the 2017 cruise (Fig. 4a). Similar distributions below the mixed layer were found for the 1994 and 2008 cruises.

Unlike surface DOC distributions, DON showed no clear trend either along the transect or between years (Fig. 3d) except for the region north of 12°S in 1994. In that year, [DON] within the mixed layer was elevated and averaged 5.5 ± 0.6 μmol kg^{-}1. Concentrations in 2008 and 2017 were similar, averaging 3.9 ± 0.5 μmol kg^{-1} and 4.0 ± 0.4 μmol kg^{-1}, respectively. Within the gyre between 12°S and 27°S, and at latitudes >27°S, [DON] within the mixed layer was similar for all years, averaging 4.2 ± 0.5 μmol kg^{-1} and 4.1 ± 0.4 μmol kg^{-1}, respectively. Below the mixed layer, DON concentrations were rather patchy, with the lowest concentrations found in the southern portion of the SPSTG at <3.5 μmol kg^{-1} (Fig. 4b).

Surface [DON] within the mixed layer did not follow the [DOC] increase inside the gyre's interior, so DOC:DON ratios varied along the P18 subsection. Considering all cruises, DOC:DON mean ratios were relatively low near the equator and in the south, but gradually increased toward the gyre (Fig. 3e). A similar trend in the ratios was previously observed by integrating the upper 30 m using the 1994 cruise data (Hansell and Waterhouse, 1997). The two linear regression lines separating the northern and southern portions of the region reflects this pattern (Fig. 3e). Outside the limits of the SPSTG, the regression lines fall below the DOC:DON mean of 15.7:1 (Fig. 3e, dashed line), but were above the mean for waters inside the gyre. The ratio averaged 15.0:1 ± 2.2 north of 15.5°S, where NO_3^- was abundant, and was 17.1:1 ± 3.2 inside the gyre when NO_3^- was below detection limit, reaching a maxima of 24:1 at 25°S. South of 35.5°S, where NO_3^- was abundant again, ratios averaged 15:1 ± 3.9.There was interannual variability in the ratio, reflecting [DOC] and [DON] fluctuations during different years (Fig.S2). The year 1994 showed the lowest ratios overall, while 2017 had the highest. However, the same pattern (i.e., lower ratio in the gyre margins, increasing toward the center) was observed during all years.

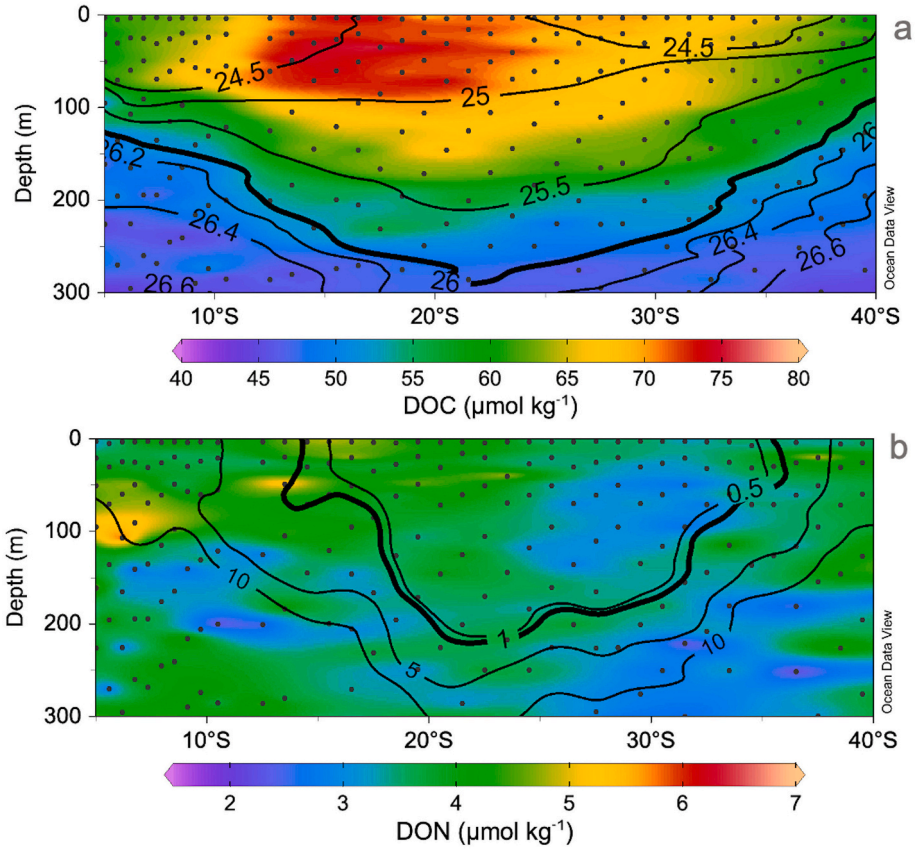

Fig. 4. Sections from the P18/2017 cruise showing (a) DOC (μmol kg^{-1}) overlain by density (σ_θ; kg m^{-3}) and (b) DON (μmol kg^{-1}) overlain by NO_3^- (μmol kg^{-1}). Black dots represent sampling effort.

3.3. Relationships between DOC and DON distributions and physical properties

To evaluate the physical controls on DOC and DON distributions, relationships with salinity and potential temperature were considered. Salinity-normalized DOC and DON were calculated to remove the effects of evaporation and precipitation. sDOC and sDON distributions were like the uncorrected observations, with increasing sDOC concentrations toward the gyre and without a clear pattern for sDON (Fig. 5a). The role of evaporation (precipitation) in concentrating (diluting) both parameters was minor, as shown by subtracting the salinity-normalized values from the uncorrected data (Fig. 5b). The maximum concentration increase due to evaporation from the equatorial and subtropical front zones toward the gyre can be estimated by considering the regions comprised within 5°S to 21.5°S and 39.5°S to 21.5°S, as these latitudes had the minimum (at 5°S and 39.5°S) and maximum (at 21.5°S) salinity values. Mean ΔDOC attributed to surface evaporation was 2.05 ± 0.05 μmol/kg^{-1} while mean ΔDON was 0.14 ± 0.05 μmol/kg^{-1}. Salinity-corrected sDOC:sDON averaged 17.6:1 (dashed gray line, Fig. 5c), slightly higher in comparison to the uncorrected DOC:DON of 15.7:1.

Neither DOC nor DON were significantly correlated with potential temperature, showing no relationship with the conservative variable as evidenced by the regression models (Fig.S3).

3.4. $\delta^{15}N$ of NO_3^- and $\delta^{15}N$ of DON

$\delta^{15}N$ of NO_3^- had similar signatures during 2008 and 2017 cruises, with highest values near the Equator and the ST front zone, never under 13‰ within the mixed layer (Fig. 6a,b; Table S1). Waters inside the subtropical gyre had undetected NO_3^- concentrations and, thus, no $\delta^{15}N$-NO_3^- data. In the nutricline, $\delta^{15}N$ of NO_3^- ranged from 2.1–13.3‰ in 2008 and 6.2–11.5‰ in 2017. There was a high correlation between co-located stations collected during different years ($R^2 = 0.86$, $p > 0.05$; Fig.S1), implying that similar biogeochemical processes reflected similar $\delta^{15}N$-NO_3^- signatures during both cruise years.

Lastly, $\delta^{15}N$-DON is shown for the 2017 cruise (Fig. 6c). Variability in the isotopic signatures is an indicator of biological processes along the path between the gyre margins toward its center. However, these signatures were also associated with water masses supplying NO_3^- to the surface waters. In the equatorial region dominated by the ESW, $\delta^{15}N$-DON averaged 3.8 ± 1.5‰ in the upper 300 m and ranged between 1.9‰ and 4.0‰ within the mixed layer, while $\delta^{15}N$ of NO_3^- averaged 15.1 ± 1.9‰ within the mixed layer (Figs. 6, 7). The isotopic signature increased within the gyre where [NO_3^-] was non-detectable, averaging 5.0 ± 0.9‰ in the upper 300 m and 5.1 ± 0.7‰ within the mixed layer. $\delta^{15}N$-DON reached the lowest values in the southern margin of the gyre dominated by ESPIW. Where NO_3^- was abundant such as at 39.5°S, $\delta^{15}N$-DON averaged 2.5 ± 1.6‰ within the mixed layer but was as low as 1‰ at the surface. In this region, $\delta^{15}N$ of NO_3^- averaged 19.7 ± 3.8‰.

4. Discussion

4.1. Interannual variability in the southeast Pacific Ocean upper waters

The region nearby the Equator dominated by ESW was the only one having a significant interannual variability between cruises. This region is considered a high-nutrient low-chlorophyll (HNLC) zone limited by iron while NO_3^- is in excess (Kolber et al., 1994; Behrenfeld and Kolber, 1999), relying on nutrient contributions from the Peru Current as well as from the equatorial upwelling system advected by SEC, both imprinting a cooler signature to the ESW (Pennington et al., 2006). Ocean-atmospheric oscillations such as ENSO play a significant role locally by changing the relative contribution of these cold waters to the ESW formation. The 1994 cruise had relatively high potential temperature, high [DOC] and [DON] and low [NO_3^-] in comparison to 2008 and 2017 cruises (Fig. 3). Because of this, we investigated whether El-Niño conditions could have controlled the variability in the physico-chemical properties during the different cruise years. The Niño 3 index (5°N-5°S,150°W-90°W) of monthly sea surface temperature anomaly (SSTA) was evaluated by calculating the mean SSTA considering the two

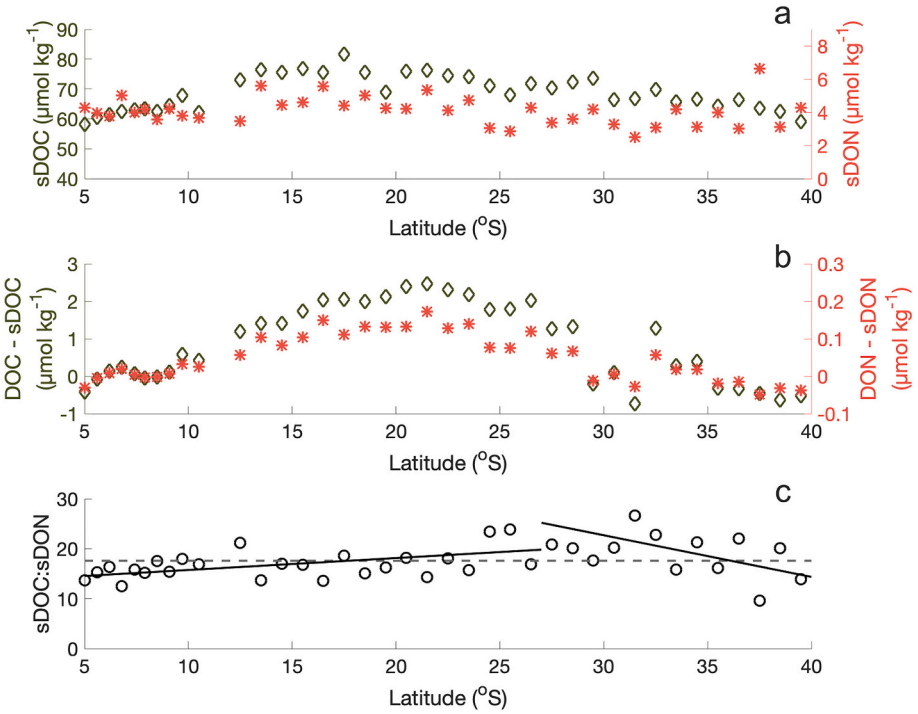

Fig. 5. Salinity-normalized distribution of DOC and DON for the 2017 cruise. (a) Mean sDOC and sDON (μmol kg^{-1}) concentrations within the mixed layer ; (b) net effect of evaporation in DOC and DON concentrations; and (c) sDOC:sDON ratios with mean ratio (dashed line) and trendlines for subsections between 5°S-32°S and 32°S-40°S (continuous lines).

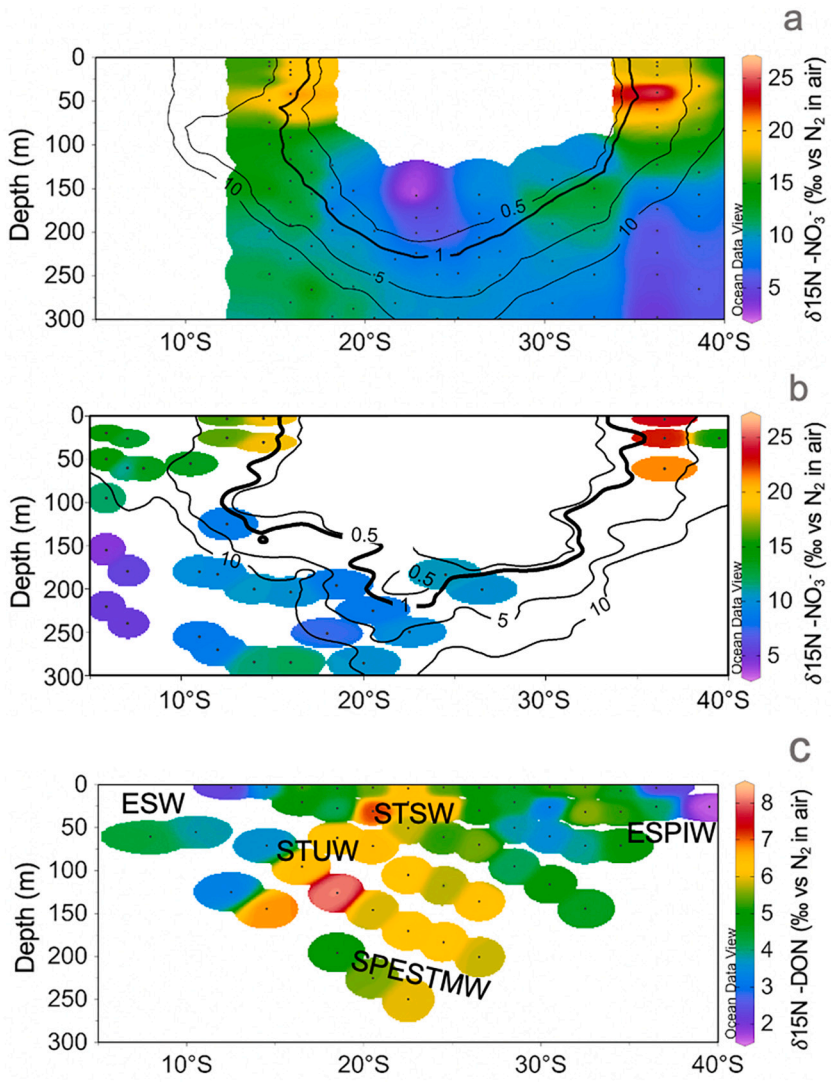

Fig. 6. Isotopic signatures for P18 cruises. (a) $\delta^{15}N$ of NO_3^- (‰) overlaid by [NO_3^-] (μmol kg^{-1}) for the 2008 cruise; (b) $\delta^{15}N$ of NO_3^- (‰) overlaid by [NO_3^-] (μmol kg^{-1}) for the 2017 cruise; (c) $\delta^{15}N$ of DON (‰) and location of main water masses for the 2017 cruise.

months preceding each cruise plus the sampling month as the final index for 1994, 2008 and 2017. Data were provided by the Global Climate Observing System (GCOS; available at https://www.esrl.noaa.gov/psd/gcos_wgsp/Timeseries/Nino3/), and the Niño 3 index was chosen as it better represented our study area (Kao and Yu, 2009).

The 1994 and 2017 cruises were sampled under neutral conditions (SSTA = −0.36 and − 0.35, respectively) while 2008 was sampled under La Niña conditions (SSTA = −1.66). Considering that 2008 and 2017 were sampled during the same season, and that 2008 was relatively colder and nitrate-enriched (Fig. 3), the variability of the different properties could have been in part explained by a higher relative contribution of cold, high-nutrient waters in 2008 (La Niña) versus 2017 (neutral conditions). However, the warmer and fresher waters enriched in DOC and DON and with low [NO_3^-] found in 1994 could not be explained by ENSO conditions observed that year. Since the 1994 cruise was sampled in a different season (Table 1), the variability in temperature and salinity could have been simply due to seasonality. At the same time, increased DOC and DON concentrations and decreased [NO_3^-] could indicate enhanced local PP at that time. Historically, chlorophyll-a concentrations and PP are significant in the region at intermediate production in comparison to the equatorial upwelling system (high production) and the subtropical gyre (low production; Pennington et al., 2006), with DOC approaching 20% of new production (Hansell et al., 1997a, 1997b). Additionally, since samples were collected unfiltered in 1994, elevated [DOC] near the Equator could have been attributed to particulate organic carbon as a result of PP. For the remaining transect there was little interannual variability except for the relatively low DOC observed South of 27°S in 1994 (Fig. 3c). Since no other properties showed significant interannual differences, other factors not assessed in this work could have affected concentrations.

Interestingly, standard deviations from mean DOC concentrations within the mixed layer were significantly higher in 1994 (Fig. 3c). The high standard deviation observed in this cruise might reflect an increase in the measurement's precision over the years, including an analytical method improvement and the implementation of the DOC reference material program in later years (Hansell, 2005; Dickson et al., 2007; Halewood et al., 2010).

4.2. DOC and DON distributions within the mixed layer: physical versus biological controls

Surface distribution of DOC and DON inside the SPSTG is physically favored by horizontal advection from the productive margins toward the gyre's center though evaporation has also been suggested to explain these increases (Letscher et al., 2013; Carlson and Hansell, 2015). Assuming the horizontal flux from 5°S and 21.5°S where minimum and

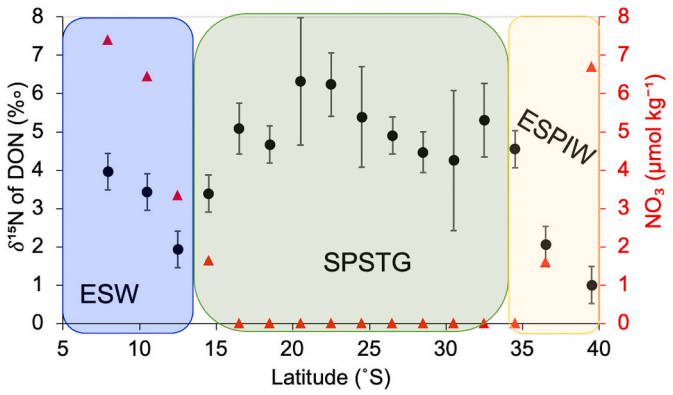

Fig. 7. Mean $\delta^{15}N$ of DON (‰) (closed black circles) and nitrate concentrations (μmol N kg^{-1}) (filled red triangles) within the mixed layer along the P18/2017 subsection. Shaded regions represent isotopic signatures and nitrate concentrations associated with the dominant surface water mass. ESW = Equatorial Surface Water (blue-shaded); SPSTG = water masses associated with the SPSTG surface waters (green-shaded); ESPIW = Eastern South Pacific Intermediate Water (yellow-shaded). Error bars are the sum of ±1 standard deviation from replicates within the mixed layer and the propagated error associated with the analysis. (For interpretation of the references to colour in this figure legend, the reader is referred to the web version of this article.)

maximum contributions from evaporation are observed respectively, a total accumulation of ΔsDOC = 18.12 μmol kg^{-1} is observed (Fig. 5a), a difference of Δ(DOC-sDOC) = 2.50 μmol kg^{-1} that can be attributed to salinity alone (Fig. 5b). Comparing these two values, the salinity effect explained about 10% of the total DOC increase inside the gyre and thus plays a minor contribution to total accumulation. On the other hand, ΔsDON was near zero considering differences between any considered latitude. Assuming DON concentrations are about an order of magnitude lower than DOC, and that the salinity effect must act on concentrating or diluting the two pools similarly, our analysis could not have been sensitive enough to detect small changes in Δ(DON-sDON) of tens of micromoles.

Surface dilution of DOC and DON through vertical physical processes such as diffusion and convective mixing act on diluting DOC and DON concentrations through exchanges with depleted underlying waters along the SPSTG. But these exchanges inside the gyre are minimal due to the high stratification and permanent and shallow pycnocline that lies beneath the upper mixed layer (Fiedler and Talley, 2006). Considering the downward DOC fluxes through vertical diffusion for example, carbon losses below the thermocline corresponds to only 2% of the primary production inside the gyre, an equivalent of 0.44 g C m^{-2} y^{-1} (Raimbault et al., 2007). For instance, the value is less than half of the exchange estimated in the Mediterranean during oligotrophic conditions at 1 g C m^{-2} y^{-1} (Avril, 2002). Similarly, DON diffusive losses correspond to ~0.024 g N m^{-2} y^{-1}, calculated from the Raimbault et al. (2007) dataset. Evaporation (precipitation) and vertical diffusion should not be major drivers controlling the observed [DOC] and [DON] distributions nor should promote significant changes in DOC:DON ratios along the region.

Previous studies reported an increase in DOC:DON ratios toward the center of the SPSTG in agreement with our study (Hansell and Waterhouse, 1997; Letscher et al., 2013). Yet, if differences in DOC and DON distributions and increasing ratio are due to biological activity, what processes accumulate DOC toward the gyre interior while keeping DON concentrations nearly constant? The SPSTG is considered an important reservoir of recalcitrant DOC (Raimbault et al., 2007), an accumulation that is observed in other oligotrophic gyres as well (Hansell et al., 2009). In the margins, a fraction of freshly-produced DOC that is not readily metabolized by heterotrophs accumulates at surface to be advected toward the gyre's center (Álvarez-Salgado et al., 2007; Raimbault and Garcia, 2008; Carlson and Hansell, 2015), while the highly-stratified interior allows minimal vertical exchanges between the surface, itself depleted in inorganic nutrients but replete in DOM, and underlying waters, nutrient-replete but DOM-deplete (Fiedler and Talley, 2006; Raimbault et al., 2007, Hansell et al., 2009, this study). The physical constraint not only limits vertical DOM dilution but also nutrient inputs, so primary production mainly relies on regenerated production (Raimbault et al., 2007; Raimbault and Garcia, 2008). To reflect our observations, DOC and DON distributions must be a consequence of high C:N DOM production from the margins toward the gyre's center and/or high consumption of advected DON over DOC, since a fraction of the latter might not be bioavailable for phytoplankton or microbes due to nutrient limitation, a process observed elsewhere (Zweifel et al., 1993; Kähler and Koeve, 2001; Raimbault et al., 2007; Repeta, 2015; Bif et al., 2018). The high residence times of the SPSTG upper waters, limited vertical mixing, high C:N DOM production and preferential consumption of DON over DOC might favor DOC accumulation to the observed values reported here, while keeping [DON] at similar levels. The DOC accumulation is also consistent between the three cruises analyzed here and extends Hansell and Waterhouse (1997) study in the region.

The role of advected DON as an additional nitrogen source to the gyre has received little attention. DON transformations are often neglected from primary productivity estimates and have not been included in biogeochemical models. While the margins are estimated to laterally supply similar magnitudes of dissolved inorganic and organic nitrogen to the gyre's center (>200 mmol N m^{-2} yr^{-1}), the inorganic form is totally depleted before reaching the center while the organic form is not (Letscher et al., 2013; Letscher et al., 2016). Other nitrogen sources such as atmospheric deposition and N_2-fixation are minimal to the SPSTG and do not constitute significant sources of new nitrogen to the system (Jickells et al., 2005; Knapp et al., 2016; Turk-Kubo et al., 2014). Thus, whether advected DON constitutes a potential source of nitrogen to the gyre's autotrophs and heterotrophs must be assessed. While microbial incubations indicated that surface DON from the eastern margin of the South Pacific was relatively resistant to heterotroph degradation inside the gyre in the timeframe of weeks (Letscher et al., 2016), DON surface distribution and differences in $\delta^{15}N$-DON between that margin and the gyre suggest the opposite, shedding light on the biological processes that must be taking place from nutrient-rich to nutrient-depleted waters (Knapp et al., 2018).

4.2.1. *Evidence of DON uptake inside the SPSTG revealed by $\delta^{15}N$-DON isotopes*

Knapp et al. (2018) investigated controls on DON concentrations in the eastern South Pacific using $\delta^{15}N$-DON in a zonal section from Chile (80°W) toward the center of the SPSTG (100°W) during two cruises in 2010 and 2011. Two of our stations are nearly co-located: 15°S, 100°W and 20°S, 100°W (Knapp et al., 2018) vs 14.5°S, 103°W and 20.5°S,103°W (this study). It is important to note that Knapp et al. (2018) found differences in [DON] and $\delta^{15}N$-DON between years at those stations during different ENSO conditions (i.e., El Niño in 2010 and La Niña in 2011), which led to local interannual variability in the upper ocean's temperature and salinity.

Although we did not observe significant changes in [DON] along the P18/2017 subsection, surface $\delta^{15}N$-DON signatures significantly increased between the gyre's margins and its center (Welch's *t*-test comparing signatures within the margins versus within the gyre, $p > 0.05$). The range of surface $\delta^{15}N$-DON along the SPSTG is comparable to other oligotrophic gyres. In the North Pacific Ocean at station ALOHA, $\delta^{15}N$-DON varied between 4 and 5‰ (Knapp et al., 2011). In the subtropical North Atlantic Ocean, $\delta^{15}N$-DON signatures ranged from 3.9‰ at BATS (Knapp et al., 2005) to 2.6‰ near the Azores Front (Bourbonnais et al., 2009). The lower $\delta^{15}N$ of DON observed in the northeast subtropical Atlantic possibly reflects the influence from N_2 fixation (values ranging from 0‰ to −3‰; Minagawa and Wada, 1986). Here we compare the range of [DON] and $\delta^{15}N$-DON from this study (Fig. 4d) and

Knapp et al. (2018) at similar latitudes, longitudes, and bottle depths from 5 m to ~100 m. At ~15°S [NO_3^-] was never depleted in either study. $\delta^{15}N$ of NO_3^- had a signature of 18.0‰ in our study versus 16.8‰ from Knapp et al. (2018), meaning the nitrogen source for DON production had similar signatures for both studies. In our assessment, [DON] ranged between 4.0 and 6.1 μmol kg^{-1} with $\delta^{15}N$-DON between 5.0 and 6.5‰, versus [DON] of 5.0–6.3 μmol kg^{-1} and $\delta^{15}N$-DON of 3.3–6.5‰ from Knapp et al. (2018) – similar values for both studies. The ~20°S station was located inside the gyre's center and [NO_3^-]-depleted. In our study, [DON] ranged between 3.7 and 4.7 μmol kg^{-1} with $\delta^{15}N$-DON between 5.0 and 7.2‰, versus [DON] between 4.0 and 5.3 μmol kg^{-1} with $\delta^{15}N$-DON between 4.2 and 4.8‰ in Knapp et al. (2018). At this location, our study showed relatively low DON concentrations with heavier isotopic signatures. Comparing the nitrate-replete versus nitrate-deplete stations, both studies observed relatively high [DON] and low isotopic signatures in the station with excess nitrate, and low [DON] with high $\delta^{15}N$-DON in the N-limited station inside the gyre.

According to Knapp et al. (2018), three processes are mainly responsible for changing isotopic ratios in the transition from DON-source regions to DON-sinks: (1) relatively low isotopic signatures can be attributed to freshly produced DON in regions with available NO_3^- but with enhanced PP such as the SPSTG margins, as exemplified above by the stations near 15°S. In that region, DON stocks are positively correlated with gross oxygen production and chlorophyll-a levels (Knapp et al., 2018). In our case, the regions dominated by ESW and ESPIW, with intermediate chlorophyll *a* levels and potentially enhanced PP (Pennington et al., 2006) contained low isotopic signatures associated with process (1) (Fig. 7). Two other processes act on increasing isotopic signatures of surface DON: 2) the production of DON from NO_3^- with an elevated $\delta^{15}N$ and 3) preferential consumption of low $\delta^{15}N$-DON.

Process (2) would increase [DON] while process 3 would decrease [DON]. Preferential consumption of low $\delta^{15}N$ of DON is supported by several studies (e.g., Hannides et al., 2013; Knapp et al., 2018; Zhang et al., 2020). The high $\delta^{15}N$ of NO_3^- in mechanism 2 could originate from isotopic fractionation during incomplete NO_3^- consumption or residual NO_3^- transported from the eastern tropical south Pacific Ocean oxygen deficient zone where subsurface denitrification occurs. However, process (2) can be disregarded when vertical distributions and isotopic signatures of $\delta^{15}N$-DON and $\delta^{15}N$-NO_3^- are assessed (Fig. 6). Assuming a scenario where vertical advection of underlying waters constituted a significant source of $\delta^{15}N$-NO_3^- to the gyre that enhances $\delta^{15}N$ of DON in relation to the margins, we would first need to assume a complete transformation of that NO_3^- into DON due to absence of [NO_3^-] above the nitracline. To elevate $\delta^{15}N$-DON signatures inside the gyre, $\delta^{15}N$-NO_3^- signatures within the gyre's nutricline should have been higher than signatures in the margins, but they are the opposite (Fig. 6ab). Additionally, a gradient in $\delta^{15}N$-DON between the mixed layer and the nitracline, with $\delta^{15}N$ -DON increasing with depth due to incomplete mixing would also be expected but is not observed (Fig. 6c). Instead, high $\delta^{15}N$-DON isotopic signatures are propagated within and below the mixed layer.

Assuming net DON advection toward the gyre, process (3) seems more plausible in explaining the elevated $\delta^{15}N$ of DON values inside the gyre. The preferential consumption of advected DON with low $\delta^{15}N$-DON, would produce high $\delta^{15}N$-DON inside the gyre without changing DON concentration if DON supply from advection is tightly coupled to DON consumption. The presence of similarly elevated $\delta^{15}N$ of DON signatures below the mixed layer suggests that the same process might be occurring deeper in the water column. Thus, advected DON must support PP inside the gyre as previous works suggested (Letscher et al., 2016; Knapp et al., 2018), producing a feature of increased $\delta^{15}N$-DON signatures in nitrate-depleted waters (Fig. 7). PP should be heavily sustained by recycled nutrients in the euphotic layer, with advected DON being an additional source of nitrogen to the oligotrophic gyre and tightly coupled with production. Independent of the dominant source of nitrogen to the SPSTG, DON consumption should be taken into consideration when looking for the missing nitrogen source to close productivity estimates.

5. Conclusions

Here we present surface data for several biogeochemical variables collected during three repeated hydrography cruises that crossed the eastern South Pacific Ocean along the P18 subsection in the years 1994, 2008 and 2017. DOC and DON showed little interannual variability within the mixed layer except in the equatorial region, associated with seasonality and ENSO variability. While surface DOC increased inside the gyre's center, no significant changes in DON concentrations were observed. These differences were reflected in the DOC:DON ratios that increased toward the gyre's center but could not be explained solely by physical processes (e.g., horizontal advection, evaporation and vertical diffusion from below). Indeed, evaporation played a small role in accumulating DOC and DON inside the gyre. ΔsDOC showed higher accumulation possibly due to production of high C:N DOM inside the gyre and limited consumption of the DOC fraction. Meanwhile, ΔsDON was variable possibly due to remineralization processes. $\delta^{15}N$-DON isotopic signatures increased from the Equator and high latitudes toward the center of the gyre indicating that biological reworking of surface DON left behind heavy isotopic signatures. These heavy signatures suggest that advected DON must comprise an additional source of nitrogen to stimulate local PP inside the South Pacific Subtropical Gyre.

Declaration of Competing Interest

None.

Acknowledgements

This work was only possible thanks to efforts made by the crew and scientists aboard the three U.S. repeat hydrography cruises, and we appreciate those who collected, analyzed, and made data available. We thank three different programs, each responsible for coordinating one P18 cruise per decade: the U.S. World Ocean Circulation Experiment (1994), U.S. Repeat Hydrography Program (2007) and U.S. GO-SHIP (2017). Cruise reports containing the methodologies for each hydrographic measurement included in this study can be found at: https://cchdo.ucsd.edu/data/5556/p18do.pdf (1994), https://cchdo.ucsd.edu/data/10318/p18_33RO20071215do.pdf (2008) and. https://cchdo.ucsd.edu/data/19799/33RO20161119_do.pdf (2017). We also thank Lilian Custals for assisting with DOC and TDN analysis. M.B·B. was supported by the Mary Roche Fellowship – University of Miami and by Dave and Lucile Packard Foundation. D.A.H. was supported by the National Science Foundation (OCE-2023500). M. B.B conceived the study, collected data (DOC and TDN, P18/2017), performed data processing and analysis, and wrote the first draft of the manuscript. D.A.H. collected data (DOC and TDN, P18/1994). A.B., J.G., H.W. and M.A. contributed with method development and data analysis of nitrogen isotopes. All authors contributed to data interpretation, manuscript discussions and edited the final draft of the manuscript.

Appendix A. Supplementary data

Supplementary data to this article can be found online at https://doi.org/10.1016/j.marchem.2022.104136.

References

Altabet, M.A., 1988. Variations in nitrogen isotopic composition between sinking and suspended particles: Implications for nitrogen cycling and particle transformation in the open ocean. Deep Sea Res. Part A. Oceanograp. Res. Paper. 35 (4), 535–554.

Álvarez-Salgado, X.A., et al., 2007. Contribution of upwelling filaments to offshore carbon export in the subtropical Northeast Atlantic Ocean. Limnol. Oceanogr. 52, 1287–1292.

Avril, B., 2002. DOC dynamics in the northwestern Mediterranean Sea (DYFAMED site). Deep Sea Res. Part II: Top. Stud. Oceanograp. 49 (11), 2163–2182.
Behrenfeld, M.J., Kolber, Z.S., 1999. Widespread iron limitation of phytoplankton in the South Pacific Ocean. Science 283 (5403), 840–843.
Berman, T., Bronk, D.A., 2003. Dissolved organic nitrogen: a dynamic participant in aquatic ecosystems. Aquat. Microb. Ecol. 31 (3), 279–305.
Bif, M.B., Hansell, D.A., Popendorf, K.J., 2018. Controls on the fate of dissolved organic carbon under contrasting upwelling conditions. Front. Mar. Sci. 5, 463.
Bourbonnais, A., et al., 2009. Nitrate isotope anomalies reflect N_2 fixation in the Azores front region (subtropical NE Atlantic). J. Geophys. Res. Oceans 114 (C3).
de Boyer Montégut, C., et al., 2004. Mixed layer depth over the global ocean: an examination of profile data and a profile-based climatology. J. Geophys. Res. Oceans 109, C12003.
Bradley, P.B., et al., 2010. Inorganic and organic nitrogen uptake by phytoplankton and heterotrophic bacteria in the stratified mid-Atlantic bight. Estuar. Coast. Shelf Sci. 88 (4), 429–441.
Bronk, D.A., Ward, B.B., 1999. Gross and net nitrogen uptake and DON release in the euphotic zone of Monterey Bay, California. Limnol. Oceanogr. 44 (3), 573–585.
Bronk, D.A., Ward, B.B., 2005. Inorganic and organic nitrogen cycling in the Southern California bight. Deep-Sea Res. I Oceanogr. Res. Pap. 52 (12), 2285–2300.
Bronk, D.A., et al., 2007. DON as a source of bioavailable nitrogen for phytoplankton. Biogeosciences 4 (3), 283–296.
Carlson, C.A., Hansell, D.A., 2015. DOM sources, sinks, reactivity, and budgets. In: Hansell, D.A., Carlson, C.A. (Eds.), Biogeochemistry of Marine Dissolved Organic Matter. Academic Press, pp. 65–126.
Casciotti, K.L., et al., 2002. Measurement of the oxygen isotopic composition of nitrate in seawater and freshwater using the denitrifier method. Anal. Chem. 74 (19), 4905–4912.
Charria, G., et al., 2008. Importance of dissolved organic nitrogen in the north Atlantic Ocean in sustaining primary production: a 3-D modelling approach. Biogeosci. Discuss. 5 (2), 1727–1764.
Deutsch, C., et al., 2001. Denitrification and N2 fixation in the Pacific Ocean. Glob. Biogeochem. Cycles 15 (2), 483–506.
Dickson, A.G., et al., 2007. Guide to Best Practices for Ocean CO2 Measurements. North Pacific Marine Science Organization, British Columbia, 191pp.
Fiedler, P.C., Talley, L.D., 2006. Hydrography of the eastern tropical Pacific: a review. Prog. Oceanogr. 69 (2–4), 143–180.
Halewood, E., et al., 2010. GO-SHIP repeat hydrography: determination of dissolved organic carbon (DOC) and total dissolved nitrogen (TDN) in seawater using high temperature combustion analysis. In: The GO-SHIP Repeat Hydrography Manual: A Collection of Expert Reports and Guidelines. IOCCP Report No. 14. ICPO Publications Series No. 134 Available online at. https://www.go-ship.org/HydroMan.html.
Hannides, C.C., et al., 2013. Midwater zooplankton and suspended particle dynamics in the North Pacific subtropical gyre: a stable isotope perspective. Limnol. Oceanogr. 58 (6), 1931–1946.
Hansell, D.A., 2005. Dissolved organic carbon reference material program. EOS Trans. Am. Geophys. Union 86, 318.
Hansell, D.A., Carlson, C.A., 1998. Net community production of dissolved organic carbon. Glob. Biogeochem. Cycles 12, 443–453.
Hansell, D.A., Waterhouse, T.Y., 1997. Controls on the distributions of organic carbon and nitrogen in the eastern Pacific Ocean. Deep-Sea Res. I Oceanogr. Res. Pap. 44 (5), 843–857.
Hansell, D.A., et al., 1997a. Predominantly vertical losses of carbon from the surface layer of the equatorial Pacific Ocean. Nature 386, 59–61.
Hansell, D.A., et al., 1997b. Horizontal and vertical removal of organic carbon in the equatorial Pacific Ocean: a mass balance assessment. Deep-Sea Res. II 44, 2115–2130.
Hansell, D.A., et al., 2009. Dissolved organic matter in the ocean: new insights stimulated by a controversy. Oceanography 22, 52–61.
Jickells, T.D., et al., 2005. Global iron connections between desert dust, ocean biogeochemistry and climate. Science 308, 67–71.
Kähler, P., Koeve, W., 2001. Marine dissolved organic matter: can its C: N ratio explain carbon overconsumption? Deep-Sea Res. I Oceanogr. Res. Pap. 48 (1), 49–62.
Kao, H.Y., Yu, J.Y., 2009. Contrasting eastern-Pacific and central-Pacific types of ENSO. J. Clim. 22 (3), 615–632.
Karstensen, J., 2004. Formation of the South Pacific shallow salinity minimum: a Southern Ocean pathway to the tropical Pacific. J. Phys. Oceanogr. 34 (11), 2398–2412.
Knapp, A.N., et al., 2005. N isotopic composition of dissolved organic nitrogen and nitrate at the Bermuda Atlantic time-series study site. Glob. Biogeochem. Cycles 19 (1).
Knapp, A.N., et al., 2011. Interbasin isotopic correspondence between upper-ocean bulk DON and subsurface nitrate and its implications for marine nitrogen cycling. Glob. Biogeochem. Cycles 25 (4).
Knapp, A.N., et al., 2016. Low rates of nitrogen fixation in eastern tropical South Pacific surface waters. Proc. Natl. Acad. Sci. 113 (16), 4398–4403.
Knapp, A.N., et al., 2018. Dissolved organic nitrogen production and consumption in eastern tropical South Pacific surface waters. Glob. Biogeochem. Cycles 32 (5), 769–783.
Kolber, Z.S., et al., 1994. Iron limitation of phytoplankton photosynthesis in the equatorial Pacific Ocean. Nature 371 (6493), 145–149.
Kujawinski, E.B., 2011. The impact of microbial metabolism on marine dissolved organic matter. Annu. Rev. Mar. Sci. 3, 567–599.
Letscher, R.T., et al., 2013. Dissolved organic nitrogen in the global surface ocean: distribution and fate. Glob. Biogeochem. Cycles 27 (1), 141–153.
Letscher, R.T., et al., 2016. Nutrient budgets in the subtropical ocean gyres dominated by lateral transport. Nat. Geosci. 9 (11), 815–819.
McCarthy, M., et al., 1998. Chemical composition of dissolved organic nitrogen in the ocean. Oceanogr. Lit. Rev. 6 (45), 932pp.
Meador, T.B., et al., 2007. Isotopic heterogeneity and cycling of organic nitrogen in the oligotrophic ocean. Limnol. Oceanogr. 52 (3), 934–947.
Minagawa, M., Wada, E., 1986. Nitrogen isotope ratios of red tide organisms in the East China Sea: a characterization of biological nitrogen fixation. Mar. Chem. 19 (3), 245–259.
Montes, I., et al., 2014. High-resolution modeling of the eastern tropical Pacific oxygen minimum zone: sensitivity to the tropical oceanic circulation. J. Geophys. Res. Oceans 119 (8), 5515–5532.
Moore, C.M., et al., 2013. Processes and patterns of oceanic nutrient limitation. Nat. Geosci. 6 (9), 701–710.
Morel, A., et al., 2010. The most oligotrophic subtropical zones of the global ocean: similarities and differences in terms of chlorophyll and yellow substance. Biogeosciences 7 (10), 3139–3151.
Oberhuber, J.M., 1988. An Atlas Based on the 'Coads' Data Set: The Budgets of Heat, Buoyancy and Turbulent Kinetic Energy at the Surface of Global Ocean. Tech. Rep. 15, Max-Planck-Institut für Meteorologie, 199pp.
O'Connor, B.M., et al., 2002. Formation rates of subtropical underwater in the Pacific Ocean. Deep-Sea Res. I Oceanogr. Res. Pap. 49 (9), 1571–1590.
O'Connor, B.M., et al., 2005. A global comparison of subtropical underwater formation rates. Deep-Sea Res. I Oceanogr. Res. Pap. 52 (9), 1569–1590.
Pennington, J.T., et al., 2006. Primary production in the eastern tropical Pacific: a review. Prog. Oceanogr. 69 (2–4), 285–317.
Peters, B.D., et al., 2018. Water mass analysis of the 2013 US GEOTRACES eastern Pacific zonal transect (GP16). Mar. Chem. 201, 6–19.
Peters, D.G., Hayes, J.M., Hieftje, G.M., 1974. Chemical separations and measurements: Theory and practice of analytical chemistry. WB Saunders Company, Philadelphia, PA.
Qu, T., et al., 2013. Subduction of South Pacific tropical water and its equatorward pathways as shown by a simulated passive tracer. J. Phys. Oceanogr. 43 (8), 1551–1565.
Raimbault, P., Garcia, N., 2008. Evidence for efficient regenerated production and dinitrogen fixation in nitrogen-deficient waters of the South Pacific Ocean: impact on new and export production estimates. Biogeosciences 5 (2), 323–338.
Raimbault, P., et al., 2007. Distribution of inorganic and organic nutrients in the South Pacific Ocean–evidence for long-term accumulation of organic matter in nitrogen-depleted waters. Biogeosci. Discuss. 4 (4), 3041–3087.
Repeta, D.J., 2015. Chemical characterization and cycling of dissolved organic matter. In: Hansell, D.A., Carlson, C.A. (Eds.), Biogeochemistry of Marine Dissolved Organic Matter. Academic Press, pp. 21–63.
Roussenov, V., et al., 2006. Does the transport of dissolved organic nutrients affect export production in the Atlantic Ocean? Glob. Biogeochem. Cycles 20 (3).
Santinelli, C., et al., 2021. Surface transport of DOC acts as a trophic link among Mediterranean sub-basins. Deep-Sea Res. I Oceanogr. Res. Pap. 170, 103493pp.
Schlitzer, R., 2019. Ocean Data View. https://odv.awi.de.
Seitzinger, S.P., Sanders, R.W., 1999. Atmospheric inputs of dissolved organic nitrogen stimulate estuarine bacteria and phytoplankton. Limnol. Oceanogr. 44 (3), 721–730.
Siegel, D.A., et al., 2002. Global Ocean distribution and dynamics of colored dissolved and detrital organic materials. J. Geophys. Res. 107 (C12), 3228pp.
Sigman, D.M., Casciotti, K.L., Andreani, M., Barford, C., Galanter, M.B.J.K., Böhlke, J.K., 2001. A bacterial method for the nitrogen isotopic analysis of nitrate in seawater and freshwater. Analyt. chem. 73 (17), 4145–4153.
Silva, N., et al., 2009. Water masses in the Humboldt current system: properties, distribution, and the nitrate deficit as a chemical water mass tracer for equatorial subsurface water off Chile. Deep-Sea Res. II Top. Stud. Oceanogr. 56 (16), 1004–1020.
Sprintall, J., Tomczak, M., 1993. On the formation of central water and thermocline ventilation in the southern hemisphere. Deep-Sea Res. I Oceanogr. Res. Pap. 40 (4), 827–848.
Thingstad, T.F., et al., 1997. Accumulation of degradable DOC in surface waters: is it caused by a malfunctioning microbial loop? Limnol. Oceanogr. 42 (2), 398–404.
Torres-Valdés, S., et al., 2009. Distribution of dissolved organic nutrients and their effect on export production over the Atlantic Ocean. Glob. Biogeochem. Cycles 23 (4).
Turk-Kubo, K.A., et al., 2014. The paradox of marine heterotrophic nitrogen fixation: abundances of heterotrophic diazotrophs do not account for nitrogen fixation rates in the eastern tropical South Pacific. Environ. Microbiol. 16 (10), 3095–3114.
Villa-Alfageme, M., et al., 2019. Distribution of 236U in the US GEOTRACES eastern Pacific zonal transect and its use as a water mass tracer. Chem. Geol. 517, 44–57.
Ward, B.B., Bronk, D.A., 2001. Net nitrogen uptake and DON release in surface waters: importance of trophic interactions implied from size fractionation experiments. Marine Ecol. 219, 11–24.
Weigand, M.A., Foriel, J., Barnett, B., Oleynik, S., Sigman, D.M., 2016. Updates to instrumentation and protocols for isotopic analysis of nitrate by the denitrifier method. Rap. Commun. Mass Spectromet. 30 (12), 1365–1383.
Williams, R.G., Follows, M.J., 1998. The Ekman transfer of nutrients and maintenance of new production over the North Atlantic. Deep-Sea Res. I Oceanogr. Res. Pap. 45 (2–3), 461–489.
Wong, A.P., Johnson, G.C., 2003. South Pacific eastern subtropical mode water. J. Phys. Oceanogr. 33 (7), 1493–1509.
Wyrtki, K., 1966. Oceanography of the eastern equatorial Pacific Ocean. Oceanogr. Mar. Biol. Annu. Rev. 4, 33–68.

Zhang, L., Altabet, M.A., 2008. Amino-group-specific natural abundance nitrogen isotope ratio analysis in amino acids. Rapid Commun. Mass Spectrom. 22 (4), 559–566.
Zhang, R., et al., 2020. Dissolved organic nitrogen cycling in the South China Sea from an isotopic perspective. Glob. Biogeochem. Cycles 34 (12) p.e2020GB006551.
Zweifel, U.L., et al., 1993. Consumption of dissolved organic carbon by marine bacteria and demand for inorganic nutrients. Marine Ecol. 101, 23–32.